PHOTON CT SCANNING OF ADVANCED CERAMIC MATERIALS

B.D. Sawicka

Atomic Energy of Canada Limited
Chalk River Nuclear Laboratories
Chalk River, Ontario, Canada K0J 1J0

W.A. Ellingson

Argonne National Laboratories
Argonne, IL 60439, USA

INTRODUCTION

Advanced ceramic materials (e.g. Si_3N_4, ZrO_2, SiC, Al_2O_3) are being developed for high temperature applications in advanced heat engines and high temperature heat recovery systems [1]. Although fracture toughness has been a constant problem, advanced ceramics are now being developed with fracture toughnesses close to those of metals [2]. Small size flaws (10-200 μm), small non-uniformities in density distributions (0.1-2%) present as long-range density gradients, and porous regions which can be seen as localized areas of slightly lower density, are critical in most ceramics. The need to detect these small flaws is causing a significant effort to be devoted towards nondestructive evaluation. Detection of "defects" such as those noted in engineering ceramics has presented problems for conventional non-destructive evaluation methods [3].

The use of computed tomographic (CT) imaging provides a means of obtaining accurate two-dimensional attenuation mappings of cross sections through an object, from which density variations can be obtained, within the limits of the contrast of the CT image [4-6]. CT imaging is undoubtedly going to play a crucial role in the development of reliable ceramic materials. Since small density gradients and small defects are to be observed, CT for industrial ceramics must provide images that have very good density resolution (i.e., high contrast, low noise) and be free from artifacts. While medical CT scanners with X-ray sources can be applied in some cases, especially for low-density materials, they have some drawbacks (see Sec. 2). Another possibility is to use isotopic sources. Sources can provide photons at various energies, and, with the choice of appropriate energy, are suitable to study both low and high-density ceramics. If monoenergetic sources are used, the images are free from beam hardening (BH) effects and artifacts. For multi-energy sources proper BH corrections can be easily introduced, since the energy spectra of isotopic sources are well known.

Preliminary CT evaluations of a selection of engineering ceramic components have been reported earlier [7], and it has been demonstrated that the use of isotopic sources in CT could play a key role in the development of reliable engineering ceramic materials. In the present paper we present photon source, low-noise CT scans performed for two large ceramic objects. The high contrast images obtained demonstrate the ability of the technique to detect and to quantify small density variations within ceramic tiles, as well as to detect internal cracks. The CT analyses are compared with the results of low-kV contact radiographic images.

PHOTON CT SCANNING FOR CERAMICS

Characterization of many ceramics (especially in the green state) can be achieved using medical scanners with polychromatic radiation. However, the use of these scanners has its drawbacks. One problem is that medical scanners use X-ray sources that have an energy which may be too low for large objects of high atomic number and/or density. Secondly, the polyenergetic radiation should be corrected for the so-called beam hardening (BH) effect [5,8,9], which might be a problem, especially if the energy spectrum of the X-ray sources is not well known. Thirdly, the geometry in medical scanners is usually fixed, and not necessarily well matched to specific industrial applications.

A CT image provides an accurate two-dimensional map of the X-ray (photon) attenuation in a cross-section of an object. This corresponds to a map of density in the measured cross section, but the two are not equal. If information about densities is needed, it is necessary to transfer the attenuation data into the density data using the known mass attenuation coefficients of the compound being studied. The measured intensity, I, for photons of energy E, is related to the linear attenuation as:

$$\mu \cdot x = \ln I_0/I \qquad (1)$$

where μ is the linear attenuation coefficient (in cm^{-1}) for a given material at energy E,
x is the distance (in cm) that the beam travels through the material,
I_0 is the measured unattenuated photon intensity,
I is the intensity of transmitted photons.

The linear attenuation coefficient μ is related to the mass attenuation coefficient, μ_m (at energy E, i.e., for a monoenergetic source), as

$$\mu_m \cdot \rho = \mu. \qquad (2)$$

The absorption coefficients are strongly energy dependent, but are known for all elements in a wide energy range [10,11] and therefore can be calculated for all materials of known compositions. For a fixed energy:

$$\mu_m \cdot \rho \cdot x = \ln I_0/I, \text{ and } \rho = (\ln I_0/I) \cdot \mu_m \cdot x. \qquad (3)$$

For a CT scan obtained with a monoenergetic source, the absolute values of the density can be obtained from measured attenuation data in a straightforward way, using the above formulas and the corresponding values of μ_m for the materials. A photon source of energy close to 1.2 MeV (e.g. Co-60) is especially convenient, because for this energy the mass absorption coefficients are the same (within 5-10%) for all elements except hydrogen, and therefore, the density data can be determined from such scans quite accurately even without advance knowledge of the chemical composition of the object.

To obtain a density map from an attenuation CT map measured using a polyenergetic source (e.g., X-rays), a transformation function has to be constructed, which integrates over all photon energies in the source and properly corrects for beam hardening (BH) effects [8,9]. The BH effects are especially strong for dense, high atomic number objects imaged by low-energy spectrum. BH correction is possible if the energy spectrum is well known, as is the case, e.g., for polyenergetic sources such as Ir-192. For CT scans obtained with X-ray sources, the transfer from attenuation data to the density data is complicated and therefore is not made in most cases, and instead, the CT images are presented relative to the standards of known densities.

A requirement for the application of CT to ceramics is that the CT images have to be measured with high contrast (i.e., low noise), since otherwise small density gradients and small flaws would not be detected. The density can be measured within each pixel of the image with an accuracy equal to the noise of the image. The pixel-to-pixel statistical noise, which determines the density resolution, depends on several factors [12]. The contrast of the CT image (i.e., the inverse of the noise) for fixed scan parameters depends on the value of the absorption coefficient (and therefore the energy of the source) and the intensity of the radiation transmitted through the object (and therefore the source intensity and the sample thickness). Thus, for industrial CT applications one would like to both optimize the photon (X-ray) energy and to increase the beam intensity. Since X-ray sources are generally more intense, the second requirement often results in X-ray sources being preferred over isotopic sources. However, for dense ceramics, especially large objects, the energy of the X-ray source may be too low to penetrate the object, in which case isotopic sources are superior.

The optimum energy choice is defined by the requirement that $\mu \cdot x = 2$, which comes directly from the formulas for the CT noise [12]. This yields an energy of about 1.25 MeV for 10 cm thick objects of both alumina (ρ = 3.95 g/ccm) and zirconia (ρ = 4.65 g/ccm) - i.e., the photon energy of a Co-60 source. In comparison, the use of an energy of 60 keV, which is about the effective energy of a 120 kV X-ray tube, decreases the signal-to-noise ratio (for the same scan parameters, source intensity and scan time) by a factor of 10 in the case of alumina, and by many (~6) orders of magnitude in the case of zirconia. For a 10 cm alumina object this increase in noise can be compensated for by using a source 100 times as intense, which is possible for an X-ray source in comparison to an isotopic source. However, for a 10 cm zirconia object a 60 keV source is simply inadequate. The lowest practical energy is about 150 keV (this corresponds to a tube voltage of ~300 kV) and even then the intensity must be a factor of 10^4 greater in comparison to the isotopic source, to compensate for the energy mismatch; for 100 keV the required increase in the intensity is 10^8, and for 60 keV, ~10^{16}. For less dense materials, the energy optimization is not as important since the signal-to-noise ratio is not strongly energy dependent over a wide energy range (provided the objects are not too small, i.e. >~1 cm). For example, for a 10 cm thick graphite object (ρ = 1.8 g/cm^3), the optimum energy is about 350 keV, but the noise conditions do not worsen greatly by the use of energies between 60 keV - 1.2 MeV.

EXPERIMENTAL METHODS AND OBJECTS FOR STUDY

Two 146 mm x 146 mm densified Al_2O_3 tiles (ρ = 3.93 g/cm^3), one 6 mm thick and one 23 mm thick, see Fig. 1, were used in this study.

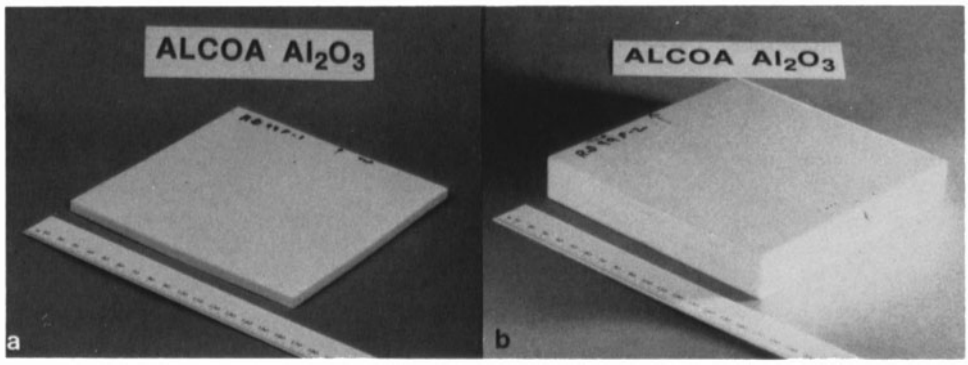

Fig. 1: Photograph of sintered Al_2O_3 ceramic tiles used for the tests. Tile sizes are 146 mm x 146 mm, with thicknesses of (a) 6 mm and (b) 23 mm.

CT tests were conducted with a first generation (translate-rotate, single detector) scanner built and operated at the Chalk River Nuclear Laboratories. The scanner consists of a gamma-radiation source (12 Ci Co-60), a CsF detector and associated electronics, a mechanical unit that rotates and translates the test object relative to the source-detector axis, and a computerized data acquisition and control system. The gamma-ray beam is collimated equally from both detector and source sides. The spatial resolution of the system is defined by the FWHM (full width at half maximum) of the beam, which can be changed to match specific applications. The performance of this scanner and its parameters have been described in detail elsewhere [13,14].

The CT images were obtained using projections sampled twice per beam width, so that the pixel (spatial element of the image) size was half of the spatial resolution, with the spatial resolution equal to the FWHM of the beam. For each image, 224 rays (beams) separated by one half of the beam width were measured for each of 360 projections. The projections were spaced 0.5° apart and spanned 180°. Two of the images were obtained using a spatial resolution of 1.92 mm FWHM (i.e., 0.96 mm pixel size), and another one with a FWHM of 1.42 mm (i.e., 0.7 mm pixel size). The CT 'slice' thickness was 1.9 mm (i.e., the FWHM of the beam in the plane of the image). The images were reconstructed using the filtered back-projection method of linearly interpolated projections with a Ram-Lak filter [6,15], and then represented in matrices of 256x256 pixels (a 224x224 image plus borders), with the pixel size equal to the ray spacing. The pixel-to-pixel statistical noise ranged from 0.5% to 1%. The use of a Co-60 photon source, which has a spectrum close to monoenergetic, assured that the images are free from beam hardening effects.

Additional non-destructive examination of the same tiles was performed by means of low-kV contact radiographic imaging, using a Picker 110 Hot-Shot X-ray imaging system. The system was operated at 70 kV and 8 mA, with a 30 inch source-to-film distance, type M-8 Ready Pack film, and a 0.002 inch Pb screen to reduce radiation scatter; the resulting film densities were 3.2.

EXPERIMENTAL RESULTS: 'THIN' TILE

Low-kV radiographs of the 6 mm thick ('thin') tile (see Fig. 2) suggested that this tile had three regions with either somewhat lower density or a change in thickness. Thickness measurements showed no appreciable change in dimension and thus the change in optical film density indicated regions of lower density of the ceramic. From the radiographs one cannot determine the absolute density to quantify the density decrease in the three regions, nor can one determine how far they extend across the tile.

CT scans for this tile were made in two planes, one parallel and one normal to the large (146 mm x 146 mm) face. Fig. 3 shows a scan taken parallel to the large face at the midplane. To expose details in density variation, this image is presented using a thresholded scale, so that the dynamic range of the scale covers only about 2% of the nominal density (i.e., densities below 3.85 g/cm^3 are presented as black, above 3.93 g/cm^3 - white, and the densities in between these limits are in various tones of gray). The three lower density regions (A, B and C) observed in the radiograph are clearly observed.

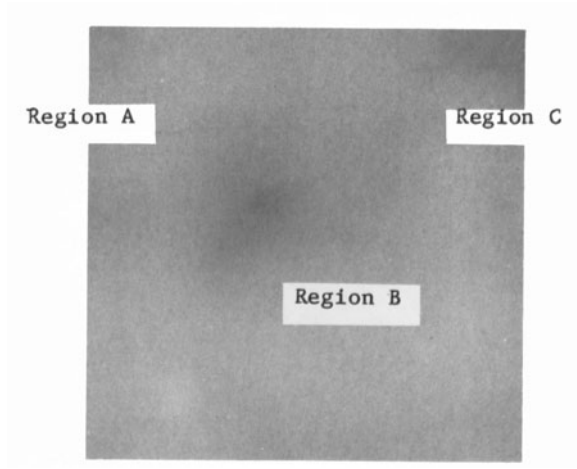

Fig. 2: Low-kV contact radiographic image of the 6 mm thick ('thin') tile.

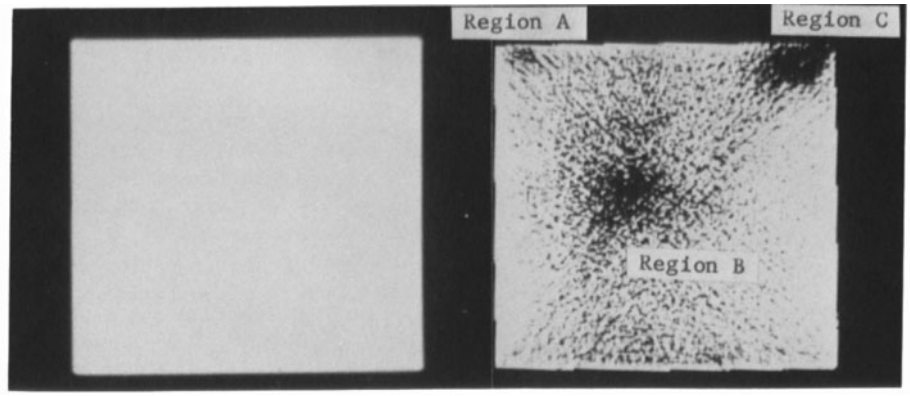

Fig. 3: CT image through the midplane of the 6 mm thick tile. The image is presented using two different linear scales: covering the whole range of densities from 0 g/cm^3 to 3.93 g/cm^3 (left image) and thresholded to encompass about 2% of the average specimen density.

To better illustrate the spatial distribution of the densities disclosed in the CT image, density profiles were plotted. Fig. 4 shows some examples of the density profile graphs, plotted along horizontal lines crossing regions A, B and C. The scale in the profiles covers a range within 20% of the maximum density (~3.3-4.1 g/cm^3). The three (A,B,C) regions are seen as corresponding dips in the graphs, from which the size of these regions can be determined, as well as the value of the density within each pixel. At the bottom of Fig. 4, are shown density profiles across the tile outside of the A, B, C regions. The vertical profile (the lowest graph) shows a scattering of the data around the average value, which reflects the statistical pixel-to-pixel noise of the image. In the horizontal profile, apart from the noise, one can also see that the density in this direction is not uniform and varies slightly but steadily from the edges to the center.

The density within each pixel can be determined to the limit imposed by the noise of the image. One can also determine the density averaged over an area enclosing a number of pixels, which can be used to decrease the error in the density determination. The average density obtained from the CT image in various locations of the tile outside of the A, B, C regions is 3.92-3.93 g/cm^3, which agrees perfectly with the nominal density of the tile determined by weighing. In regions A, B and C, the average densities determined from the CT image over an area of 10-20 pixels were 3.87 g/cm^3, 3.81 g/cm^3 and 3.84 g/cm^3, respectively, with an uncertainty of less than ±0.01 g/cm^3. The three low-density regions have therefore a density that is lower than the nominal density of the tile by, correspondingly, 1%, 3%, and 2%. Very close to the A, B, C regions the density is 3.91 g/cm^3, slightly below the nominal density of the tile. Because the tile material is chemically uniform, one concludes that the A, B and C regions indicate porous regions, with an average porosity of about 1%, 3% and 2%, for the three regions.

To examine the density variation through the thickness of the tile a cross-sectional CT scan was made across region B, along the scan line shown in Fig. 4, middle image. For this scan the pixel size was 0.7 mm. Fig. 5 shows the image of this cross section (6 mm x 146 mm), and the density profile along a horizontal line through the center of the image. The data show that the low-density B region extends throughout the thickness of the sample and is not just in the midplane displayed in Figs. 3,4.

EXPERIMENTAL RESULTS: 'THICK' TILE

Visual examination of the 23 mm thick tile showed significant cracking (see Fig. 1b). Not known was the depth to which the cracking extended, or whether the cracking was caused by a significant density gradient in the specimen. Before CT imaging this tile, low-kV contact radiographic images had been obtained (Fig. 6). Again cracks are detected, but the depths are unknown. A CT image was obtained at the midplane of the 23 mm thick tile, as for the 6 mm thick tile. Fig. 7 shows the CT image using two different gray scales, one that covers the full density range and another one that covers about 10% of the maximum density (i.e., densities below 3.7 g/cm^3 are black, above 3.95 g/cm^3 are white). The density profiles are shown in Fig. 8.

From the CT image, densities in various regions of the tile were calculated as before. The density is generally higher at the edges of the tile, 3.93 g/cm^3, and decreases towards the centre, forming two large, well separated areas of lower density (3.75 g/cm^3 at the rims of these

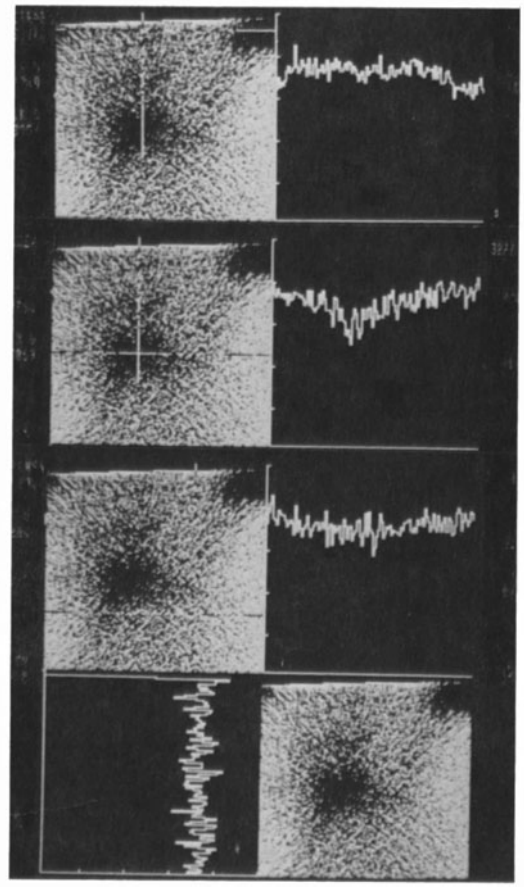

Fig. 4: Density profiles of selected locations on the 6 mm thick tile. The profiles are drawn along the lines superposed on the image and cross the low-density regions, A and C (cf. upper right graph) and B (middle right graph). The bottom image is shown with two density profiles outside the A, B, C regions, the horizontal (lower right graph) and vertical (lower left).

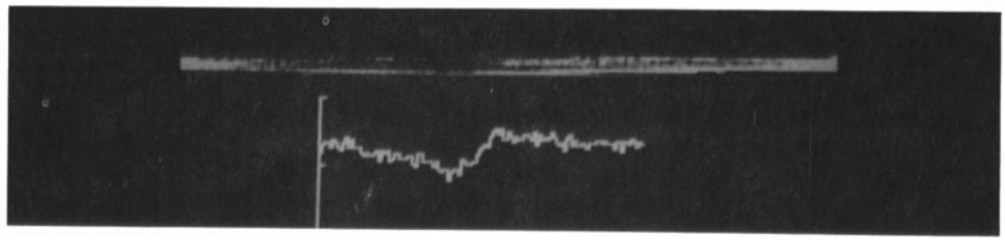

Fig. 5: CT image of the cross-sectional CT scan (i.e., taken along scan line shown in Fig. 4, middle image). The gray scale presenting the densities in the image is thresholded to cover only about 3% of the maximum density. The horizontal density profile across a part of the image (graph below) shows the extension of the low-density region. The scale of the graph covers 8% of the density range (~3.7-4.1 g/cm^3) which allows one to show both the low density B region and a long range, small (~1%) density gradient along the tile cross section.

regions and 3.67 g/cm^3 in their centers); these two regions are separated by an S-shape ribbon of denser material. The high density ribbon is quite narrow in the center of the tile (5 pixels, i.e., 5 mm or less), and it widens towards the edges of the tile to about 10 pixels (9 mm) at one end and to about 22 pixels (21 mm) at the other end (respectively right and left sides in the image in Fig. 7), at positions where it merges with the denser, edge regions (i.e., about 1 cm from the edge of the tile). At the side of this larger widening there is a crack, seen in the CT image as running along the high density ribbon, roughly in the middle, for about 4 cm. The crack width is seen in the CT image as 3 pixels wide, but in reality it is narrower than the width of one pixel. The real width of the crack was determined from the CT image by assessing the decrease in the value of the absorption coefficient in the area enveloping the crack relative to the area without the crack, and is estimated to be about 0.4 mm.

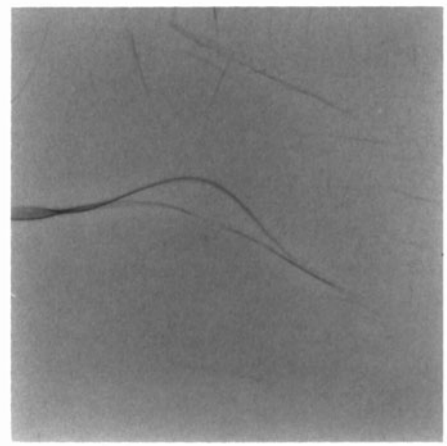

Fig. 6: Low-kV contact radiographic image of the 23 mm thick tile.

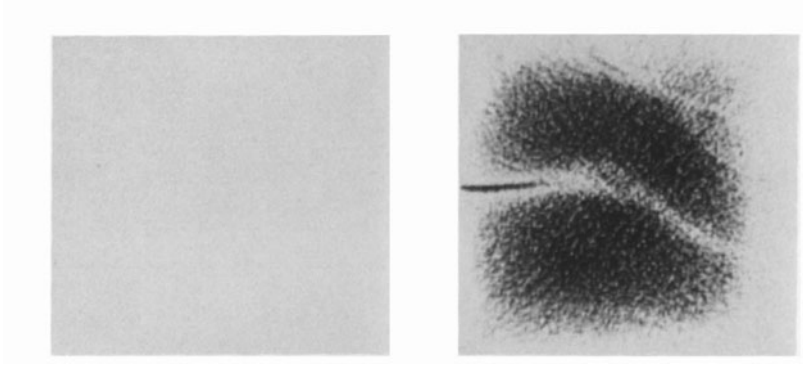

Fig. 7: CT image of the 23 mm thick tile, displayed using a scale that covers a density range 0-4 g/cm^3 (left image) and a density range from about 3.7 g/cm^3 to 3.95 g/cm^3 (right image).

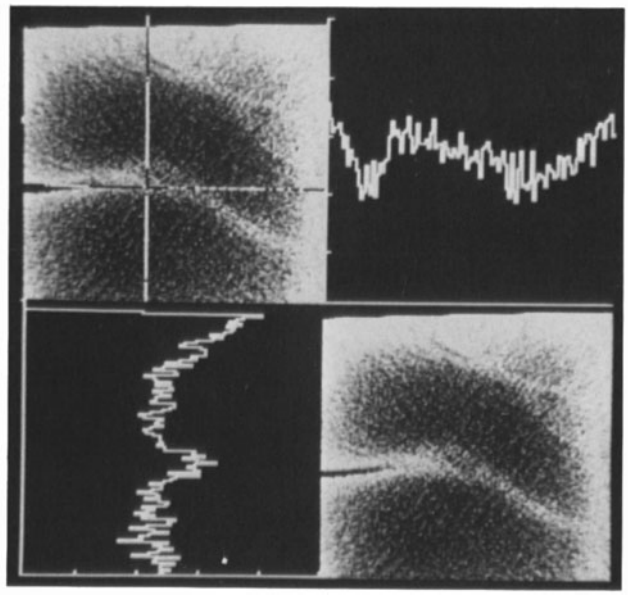

Fig. 8: Density profiles for the CT image presented in Fig. 7. The image is repeated twice, the upper one with cross-hairs along which horizontal and vertical density profiles are shown in the upper and a lower graphs respectively. The scale of the graphs covers the range of 20% of the average specimen density, i.e., ~3.3-4.1 g/cm^3.

From the CT image presented one cannot determine precisely where the crack ends. However, the low-kV contact radiograph shows this quite well (see Fig. 6). In the CT image the crack is clearly seen as long as the dense 'ribbon' around it is wider than several pixels, i.e., a length of about 4 cm. Where the 'ribbon' narrows to less than a width of 3-4 pixels, the crack cannot be seen, probably because its artificially blurred-out width coincides with the width of the high density 'ribbon'. The 'ribbon' density determined from the CT image is from 3.75 to 3.80 g/cm^3 in various places. If the crack extends further than 4 cm through the 'ribbon', then this value is artificially lowered in the CT data by the presence of the crack, and the real density is higher (e.g., if the crack runs through the narrow part of the 'ribbon' then the density in this region would be ~3.9 g/cm^3 for a crack width of about 0.2-0.4 mm). To see how far the crack extends and to confirm the above numerical data using CT imaging will require higher spatial resolution at similar contrast.

A second crack is just detectable over the noise in the CT image, in the lower density region above the high density 'ribbon'. A third crack appears to be present near the upper edge of the upper low density region, associated with another high density 'ribbon'.

A comparison of the CT image (Figs. 7,8) with the low-kV contact radiograph (Fig. 6) shows several interesting features. First, the three cracks observed in the CT image are more clearly observed in the radiograph (indicating that a higher CT spatial resolution is desirable). The tomograph locates the cracks in the mid-plane. Second, the low-kV radiograph is not as sensitive to density gradients as the CT image which shows that the cracks lie along high density 'ribbons'. Third, the small cracks in the radiograph are not visible in the CT image. Either these cracks

are not located in the midplane or the resolution of the CT image is too low.

CONCLUSIONS

Computed tomography (CT) using a high energy (1.25 MeV) photon source has been employed to image two specimens of sintered alumina ceramic. Because a monoenergetic source was used the absolute values of the densities could be measured to a high accuracy. High contrast (low noise) CT images were obtained permitting density measurement within each pixel to be determined with an accuracy of better than 1%. The average densities in regions encompassing several pixels have been determined with an accuracy of 0.2%. Porous regions and long-range density gradients were observed and quantified. Higher spatial resolution and still better contrast of the CT image could be obtained, however at the expense of the scan time. Good agreement was obtained for the two imaging techniques (CT and contact radiography), although both techniques showed slightly different features in the objects under study and therefore complement each other.

ACKNOWLEDGEMENT

The authors wanted to acknowledge the cooperation of Dr. John Weyand, ALCOA Inc., in providing the samples, and P.W. Reynolds for technical assistance in performing CT scans, and C.J. Allan for his interest and support in this work.

REFERENCES

1. D.R. Johnson, A.C. Schatthauser, V.J. Tennery, E.L. Long (Jr), and R.B. Schultz, "The Ceramic Technology for Advanced Heat Engine Project", Proc. 22nd Automotive Technology Development Contractors, published by the Society of Automotive Engineering, Warrendale, PA, March 1985 (Report ISBN 00-89883-712-2, pp. 369-377).
2. A.R.C. Westwood and J.P. Skalny, J. Advanced Ceramic Materials, 1, 21 (1986).
3. W.A. Ellingson, R.A. Roberts and M.W. Vannier, Proc. XVth Symposium on Nondestructive Evaluation, South-West Research Institute, San Antonio, Texas, 1985.
4. G.T. Herman, "Image Reconstruction from Projections", Academic Press, N.Y. (1980).
5. R.A. Brooks and G. Di Chiro, Phys. Med. Biol. 21, 689 (1976).
6. A.C. Kak, Proc. IEEE 69, 1245 (1979).
7. T. Taylor, W.A. Ellingson and W.D. Koenigsberg, Atomic Energy of Canada Limited report AECL-9005 (1985), and Ceramic Eng. and Science Proc. (in print, 1986).
8. E. Segal and W.A. Ellingson, to be published in the Proc. of the 2nd International Symposium on the Nondestructive Characterization of Materials, Montreal, July 1986, Plenum Publ.
9. P.D. Tonner, G. Tosello, D.S. Hall, L.R. Lupton and B.D. Sawicka, Atomic Energy of Canada Limited report (in preparation).
10. E. Storm and H.I. Israel, Nucl. Data Tables 7, 565 (1970).
11. W.M.J. Veigele, Atomic Data Tables 5, 51 (1970).
12. D.A. Chester, S.J. Riederer, N.J. Pelc, Journal Comp. Assist. Tomography 1, 1 (1977).
13. P.D. Tonner and G. Tosello, Materials Evaluation, 44, 203 (1986).
14. T. Taylor and L.R. Lupton, Nucl. Inst. & Meth., A242, 603 (1986).
15. G.N. Ramachandran and A.V. Lakshminarayan, Proc. Natl. Acad. Sci., USA 68, 2236 (1971).

DISCUSSION

Mr. Notea: I would like to refer to the optimization that you showed at the beginning of your talk. This optimization is correct only for cylindrical objects. Generally the function depends on the shape of the object, and also on the number and shape of the holes and the inclusions inside the object. In the Moscow meeting in 1982 it was shown that the optimum energy might be not for $\mu \cdot x = 2$ but for $\mu \cdot x$ equal 3 or 4.

Ms. Sawicka: I agree that the relation between the noise of the CT image and the product of μ times x (absorption coefficient times object thickness) depends on the shape of the object. Also the noise varies across the cross section of the object, depending on the object shape, which I neglected in my discussion. But these factors do not change the noise estimate greatly, which means that although the noise estimate from my curves may be not exact in all the cases, it is good, let us say, to within a factor of 2 or 3, and certainly within less than an order of magnitude. On the other hand, the improper choice of the energy in the case of dense objects can increase the noise by orders of magnitude, even many orders of magnitude. If this increase is not too large, up to 2 to 4 orders of magnitude, it can be compensated for by the use of much stronger sources, but there is a limit when this is possible. This is what my curves were supposed to show.

From the Floor: What is the thickness of the section that you are imaging?

Ms. Sawicka: The "in-slice" thickness in our current scanner can be changed depending on the specific application. It is determined by the half maximum of the beam width and therefore by the source size and the aperture of the collimators. For the images that I have shown here, the "in-slice" thickness was about 1 mm for the case of the green alumina pellets, and 2 mm for the CT images of the sintered tiles.

From the Floor: What is the size of your isotopes?

Ms. Sawicka: The geometrical size of the sources?

From the Floor: Yes.

Ms. Sawicka: Sources are delivered packed in small containers. The Co-60 source of required activity consists of many small pellets packed into a cylindrical container, with the circular base having the diameter of 4 mm; in our scanner this circular end is facing the detector. Ir-192 consists of several pellets stacked one behind the other, and the active area is again circular with the diameter of 3 mm. The size of the active area imposes a limit on the beam width used for the CT scans and on the possible "in-slice" thickness.

Mr. William Friedman, Standard Oil: High-aspect ratio objects sometimes produce artifacts inside the objects. Are certain generation scanners better for looking at those types of objects? Does the arrangement of the detectors and the source tend to reduce those problems?

Ms. Sawicka: It seems that the first generation scanners, which have a pencil beam and one detector, have better defined beam geometry and therefore should have less artifacts than scanners that use a fan beam and many detectors. In multidetector systems one has

to very carefully suppress the scattering which may cause artifacts. If this is properly done, perhaps there is no preference. Does anybody want to comment on this?

From the Floor: With one detector you have less scattering, so perhaps for a high-aspect ratio object, upon the significance of the scattering (cross-talk between the detectors), a first generation machine might be better. On the other hand, multidetector machines are much faster, so you gain the speed.

Mr. Segal: If you have 10 detectors instead of one, the speed is 10 times better.

Ms. Sawicka: You gain the speed but you do not decrease the artifacts, and, in machines of higher generations, perhaps increase the number of artifacts. The artifacts may arise due to both scattering between the detectors (cross talk) and scattering in the object, and both can be larger in higher generation scanners in comparison to the first generation machines. Probably the second generation scanner would be a good option.

Mr. H. Ringermacher, United Technologies Research Center: What is a typical time of acquisition of all the data you need?

Ms. Sawicka: I waited for this question. (Laughter). How many detectors?

Mr. Ringermacher: I knew you waited for it.

Ms. Sawicka: The acquisition time depends on many factors, namely the noise you allow in the CT image (whether you want a high contrast or a low contrast image), the number of detectors and the source strength you use in your scanner, the number of rays and projections you take to generate the image and the required spatial resolution. The images which I have shown today were measured with high contrast (low noise). In the case of the green pellet, the acquisition time per ray was 8 sec., and the total time was 8 sec times 90 projections times 64 rays, which gave 12.8 h, because one-detector system was used. The first generation scanner is not fast! Using 64 detectors, the acquisition time could have been reduced to 12 minutes. Our source at the time of these measurements was not very strong. We could have used a source about 7 times stronger, which would give you a 2 minute scan. This is assuming you have 64 detectors. If you are using one detector, the time is 64 times longer.

Mr. Ringermacher: In the case of the plate what did it take to do?

Ms. Sawicka: In the case of the plate the image was generated using 224 rays and 360 projections, which--with the use of 224 detectors which is quite possible to be implemented--the acquisition time would be 14 minutes. The source was Co-60, and we could have used Ir-192, which is stronger and would reduce the time by about a factor of 10, which gives less than 2 min. Again, one detector gives you the time...

Mr. Ringermacher: 224?

Ms. Sawicka: Yes, that many times longer. One more remark. The acquisition times that I quoted were required to generate the images with the noise much lower than 1%. In most cases, images having the noise 3 times larger are sufficient, and those can be generated in a time 9 times shorter in comparison to the quoted numbers.